PHYSICAL REVIEW B VOLUME 54, NUMBER 17 1 NOVEMBER 1996-I

Simulation of magnetovolume effects in ferromagnets by a combined molecular dynamics and Monte Carlo approach

Bruno Grossmann and Denis G. Rancourt*
Department of Physics, University of Ottawa, Ottawa, Ontario, Canada K1N 6N5

(Received 31 May 1996)

We present a combined molecular dynamics and Monte Carlo simulation method that treats the vibrational and magnetic degrees of freedom on an equal footing in calculating the equilibrium properties of magnetovolume-coupled local moment systems. We apply this method to a simple model system, a single-species ferromagnet with nearest-neighbor-only interatomic Lennard-Jones potential and nearest-neighbor-only intermoment Ising interactions, and calculate the relevant equilibrium properties. Some results occur that are not predicted by previous calculations that use mean-field or Landau-type approximations.

[S0163-1829(96)01342-2]

I. INTRODUCTION

Within local moment models, any ferromagnet in which the intermoment magnetic exchange parameter J depends on the intermoment separation r will exhibit spontaneous (i.e., zero applied field) magnetovolume effects. Depending on the sign of the magnetovolume coupling parameter $\partial J/\partial r$, the ferromagnet either contracts or expands when magnetic order sets in below and around the Curie point T_C. The most well-known example is classical Invar [quenched face-centered-cubic (fcc) $\mathrm{Fe}_{65}\mathrm{Ni}_{35}$] where magnetovolume coupling gives rise to its near zero thermal expansion coefficient in a broad range around room temperature.[1–4] Other recent examples of materials in which magnetovolume coupling is important include giant magnetoresistive perovskites[5,6] and diluted magnetic semiconductors.[7]

In the context of local moment ferromagnets, the general problem is a difficult one because both magnetic and phonon excitations must be treated simultaneously and on an equal footing in terms of the energies involved. The cooperative magnetic behavior arising from the ferromagnetic interactions and the thermal expansion arising from the asymmetry in the interatomic potential occur simultaneously and affect each other. They are coupled in a nontrivial manner and are not simply additive, as is often assumed in phenomenological models and in analyzing experimental data. The two components (magnetic and phonon) cannot be separated and solved independently.

The local moment formalism dealing with magnetomechanical effects, including magnetovolume, magnetoelastic, and anisotropic effects such as magnetostriction, has been developed by Callen and others.[8–15] Magnetovolume effects in general, by local moments and other mechanisms, have been reviewed by Lee[16] and more recently by Campbell and Creuzet.[17] The concomitant contributions from both local moments and itinerant electrons to magnetovolume effects in metallic magnets has been discussed and elucidated by Holden *et al.*[18] and by Moriya and Usami.[19] The latter works show that purely local moment effects dominate the magnetovolume behavior in strong local moment systems such as iron and nickel, which are known to have large local moments persisting far above their magnetic ordering temperatures.

With actual calculations, past work on magnetovolume phenomena has usually not been extended beyond average uniform lattice expansion (as expressed simply by the sample volume or, more completely, by the strain tensor) in a single-component magnet whose decoupled magnetism is treated by mean-field theory or in the context of a Landau-type expression for the free energy that includes some terms from the decoupled phonon system.[8–14,18–24] The Landau approach has also been used to study magnetovolume and magnetoelastic effects in systems exhibiting helimagnetism,[25] a spin-Peierls transition,[26] quasi-one-dimensionality,[27] a sinusoidally modulated phase,[28] and a spin-density-wave phase.[29,30]

Typically,[20] the magnetism is calculated *in vacuo* for a given fixed volume. The resulting magnetic internal energy is included in a macroscopic expression that includes a volume-dependent chemical cohesive energy, and magnetic and vibrational entropy terms, but not the vibrational kinetic energy. Each term in the free energy is then calculated as though the magnetic and phonon systems could be separated. This free energy is then minimized to obtain the sample volume as a function of temperature. Here, only a select few of the phenomenological parameters contained in the free energy (compressibility, Debye temperature, normal thermal expansion coefficient, etc.) are allowed to exhibit their intrinsic volume, pressure, and temperature dependences.

Except for some interesting but limited work in one dimension (1D),[31–35] some Monte Carlo (MC) simulations that do not include atomic vibrations,[36,37] and renormalization-group calculations that examine behavior in the critical region,[38] no microscopic calculations or simulations have been performed that use only microscopic parameters and allow complete microscopic freedom and local response to wide ranging changes in temperature, pressure, and applied field.

Here, we present a microscopic approach which combines molecular dynamics (MD) simulation for the atomic vibrations and MC simulation for the magnetic excitations, treated in the Ising approximation. We apply this method to a simple model system, a nickel-like fcc single-species local-moment ferromagnet with nearest-neighbor-only interactions. Our simulations yield new quantitative predictions and qualitative features related to magnetovolume effects.

Our method for the composite simulation is based on the experimental fact that, in most real situations, the moment (or spin) autocorrelation time is much larger than the period for typical atomic vibrations.[31,39] That is, in the average time between successive spin fluctuations on a given moment, the moment-bearing atom experiences many (10^2–10^5) atomic vibration cycles. As a result, the magnetic and vibrational events can be partially separated in time on a microscopic scale without any loss of generality, at least for simulating equilibrium properties. Of course, the kinetics would depend in detail on how this separation is applied.

In practice, the intermoment interaction for a given spin pair is sensed on the time scale of the spin autocorrelation time and, therefore, depends only on a vibrationally averaged interatomic distance instead of on the instantaneous one. On the other hand, the total force on a given atom has a magnetic component that has an instantaneous dependence on the interatomic separations. The latter force is sensed on a time scale that is small compared to the time that a particular spin configuration, on the moments within a sphere of influence, lives.

II. HAMILTONIAN AND SIMULATION ALGORITHM

The Hamiltonian contains both the magnetic energy and the elastic energy:

$$\mathcal{H}=\mathcal{H}_m+\mathcal{H}_e\,. \tag{1}$$

We chose a simple Lennard-Jones potential to model the elastic energy:

$$\mathcal{H}_e=\sum_{\langle \mathrm{NN}\rangle} 4\epsilon\left[\left(\frac{\sigma}{r_{ij}}\right)^{12}-\left(\frac{\sigma}{r_{ij}}\right)^{6}\right]. \tag{2}$$

Even though this potential is not a realistic one for transition metals and their alloys, it should mimic quantitatively well the structural properties of our nickel-like model system, provided we choose ϵ and σ appropriately. The sum is taken on nearest-neighbor (NN) atoms.

Let us now elaborate on the part of the Hamiltonian dealing with the magnetic energy. Within local moment models, the isotropic magnetovolume effect arises because the magnetic coupling constant depends on the spacing between the atoms on which the spins reside. Thus, we can write

$$\mathcal{H}_m=-\sum_{\langle \mathrm{NN}\rangle} J_{ij}\frac{\mu_{\mathrm{Ni}}^2}{4\mu_B^2}\sigma_i\sigma_j\,. \tag{3}$$

Here J_{ij} is the magnetic coupling constant which depends on r_{ij}, σ_i and σ_j are neighboring Ising variables ($=\pm 1$), μ_B is Bohr magneton, and $\mu_{\mathrm{Ni}}=0.6\mu_B$. Again, the sum is on nearest neighbors.

We do a Taylor expansion of the magnetic coupling constant around r^0, the equilibrium atomic spacing at $T=0$:

$$J_{ij}\simeq J^0+J'(r_{ij}-r^0), \tag{4}$$

with

$$J^0=J_{ij}\big|_{r^0} \tag{5}$$

and

$$J'=\left.\frac{\partial J_{ij}}{\partial r}\right|_{r^0}. \tag{6}$$

We then substitute this expression into our Hamiltonian to obtain

$$\mathcal{H}=-\sum_{\langle \mathrm{NN}\rangle} J^0\frac{\mu_{\mathrm{Ni}}^2}{4\mu_B^2}\sigma_i\sigma_j-\sum_{\langle \mathrm{NN}\rangle} J'(r_{ij}-r^0)\frac{\mu_{\mathrm{Ni}}^2}{4\mu_B^2}\sigma_i\sigma_j+\sum_{\langle \mathrm{NN}\rangle} 4\epsilon\left[\left(\frac{\sigma}{r_{ij}}\right)^{12}-\left(\frac{\sigma}{r_{ij}}\right)^{6}\right]. \tag{7}$$

In order for this Hamiltonian to be as realistic as possible, the values used for the various parameters were either directly taken or extrapolated from experimental data for nickel, when possible. The measured cohesive energy allows us to set $\epsilon=11.8595\times 10^{-20}$ J (8590 K). The equilibrium lattice parameter obtained from x-ray diffraction sets $r^0=3.524$ Å. Finally, $J^0=0.9664\times 10^{-20}$ J (700 K) is inferred from the Curie point of nickel, assuming $J'=0$ and using MC simulations.[3]

Since, as mentioned above, spin flips occur on a different time scale from atomic motion, it is natural to separate the simulation of the whole Hamiltonian into two parts. Thus we introduce the following procedure. We, for example, first perform n_{MD} MD time steps on the atomic positions alone with the full Hamiltonian [Eq. (1)] but with the spins in frozen orientations. Equilibrium average atomic positions [and associated average interatomic separations $r_{ij}(1)$] corresponding to the preset spin-structure-1 result. These $r_{ij}(1)$ are used to determine new J_{ij} values, $J_{ij}(1)$, using Eq. (4) where J^0 and J' are user defined. Then, we perform n_{MC} MC time steps on the spin system alone using $\mathcal{H}_m$ [Eq. (3)] but with the new $J_{ij}(1)$ values. There results an equilibrium spin-structure-2 corresponding to the preset $r_{ij}(1)$. Next, n_{MD} MD time steps are again performed, with frozen spin-structure-2, to give $r_{ij}(2)$ and $J_{ij}(2)$, and so on until neither the bulk magnetization or the average atomic separation change and overall equilibrium is attained. In this procedure, one step corresponds to n_{MC} MC time steps and n_{MD} MD time steps. We made several checks to insure that the results did not depend on the choice of n_{MC} and n_{MD}.

III. SIMULATION DETAILS

The MC simulations were performed using a standard spin-flip algorithm.[40] The method goes as follows: A spin is chosen at random, and the program tries to flip its sign. If the total energy is lowered through this procedure, the spin is flipped. If the total energy is increased, then the spin is flipped according to the probability distribution $\exp(-\Delta E/k_BT)$, where ΔE is the energy difference between the two configurations, k_B is Boltzmann's constant, and T is the temperature.

For the MD part, we used a constant temperature, constant pressure algorithm.[41,42] Only this type of algorithm allows us to look at magnetovolume effects in a straightforward fashion. In a standard MD algorithm, the motion of the atoms is calculated by numerically integrating the acceleration they are subjected to over time. The acceleration itself is calculated from the interatomic forces.[43] In the case of the constant pressure algorithm, the method roughly goes as follows.[44] The atoms are thought of as moving in an elastic medium which can be expanded or contracted at will. This medium has an effective mass M which is set so that the motion of the atoms cannot exceed the phonon speed of the system. It is by this expansion-contraction procedure that the average pressure is kept constant. The pressure itself is the sum of the static pressure—the pressure due to the interatomic forces—and the dynamic pressure—the pressure due to the motion of the atoms. Using this algorithm, we can also apply a pressure on the system to explore different parts of the phase diagram.

Because our simulations involved temperature ramps, care was also taken so as to avoid a biasing in the thermal expansion data. This biasing is due to the fact that, as the temperature increases, the average atomic velocity also increases. Because of the finite time step used in the simulation, this causes the round-off errors on the integrated atomic trajectories to increase. To minimize this effect, we scaled the time step used in our simulation by a factor $1/\sqrt{T}$. We checked our preliminary results by decreasing the time step and verifying that we obtained the same results.

The simulation program went as follows. The initial MD time step was taken to be $\Delta t = 5\times10^{-15}$ s. The effective mass used in the constant pressure MD algorithm was taken to be $M = 1\times10^{12}$ kg m^{-4}. Finally, n_{MD} and n_{MC} were both chosen equal to 25. Starting from a ferromagnetically aligned spin configuration on a fcc lattice, the system was equilibrated for 40 steps ($n_{\mathrm{MC}} = 40\times25 = 1000$, $n_{\mathrm{MD}} = 1000$) at the lowest temperature of the temperature ramp. For the next 200 steps ($n_{\mathrm{MC}} = 200\times25 = 5000$, $n_{\mathrm{MD}} = 5000$), the magnetization, the energy, and the average lattice parameter were recorded. We then increased the temperature and repeated this procedure. This allowed for a better equilibration of both the spins and the atomic positions, since the initial configuration was closer to the equilibrium one. In the special case of the $T = 0$ simulations, we used the standard relaxation technique, which consists in letting the atoms go to their equilibrium positions.

Most of the simulations were performed on a $10\times10\times10$ cell, which is equivalent to 4000 atoms and spins on the fcc lattice. Finite-size effects were investigated by simulating with various system sizes with the same parameters. Figures 1 and 2 show results from simulations of a $5\times5\times5$ cell, an $8\times8\times8$ cell, a $10\times10\times10$, cell and a $12\times12\times12$ cell with $J' = 1\times10^{-9}$ J m^{-1}. As can be seen from these two figures, finite-size effects for the magnetization and the average lattice parameter are only important for the smallest lattice.

As for the rounding-off effects related to the use of a finite time step in the integration procedure, Fig. 3 shows the average lattice parameter data for three different values of the time step for a $10\times10\times10$ system with $J' = 1\times10^{-9}$ J m^{-1}. Notice that even if the largest Δt value yields a curve which is quantitatively different, it still yields the same expansion coefficient as the simulations with the smaller Δt values. This allows us to conclude that the scaling of Δt is effective in canceling out the above-mentioned biasing effects due to the increase in temperature. Nevertheless, we still used the intermediate time step in our simulation to get as quantitatively accurate data as possible.

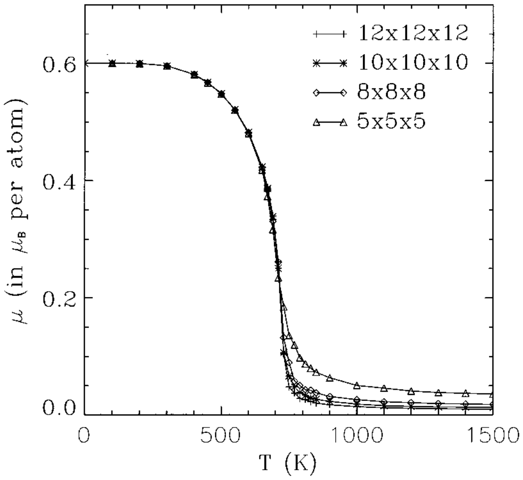

FIG. 1. Spontaneous average magnetic moment per atom as a function of temperature for various cell sizes (as indicated, in units of the fcc conventional unit cell lattice parameter) with periodic boundary conditions and $J' = 10^{-9}$ J/m.

IV. RESULTS

Figure 4 shows the zero-pressure spontaneous (i.e., zero applied magnetic field) average magnetic moment per atom (or magnetization), μ, as a function of temperature, for different values of the magnetovolume coupling parameter J'. A value of $J' = 10^{-9}$ J/m $\simeq 10^{4}$ K/Å is typical of what is required to explain the ground-state magnetovolume anomalies in classical $\mathrm{Fe}_{65}\mathrm{Ni}_{35}$ Invar.[45] We see that the Curie temperature itself is significantly affected by the value of J'. This is also shown in Fig. 5 where the zero-pressure T_C obtained from the maximum in the specific heat is plotted as a function of J'. This method for obtaining T_C gave a suffi-

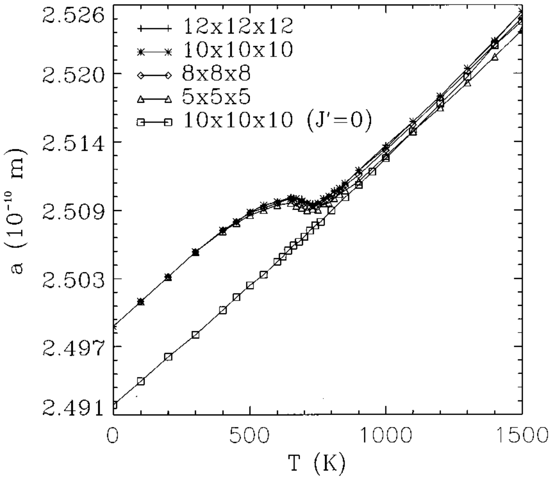

FIG. 2. Equilibrium lattice parameter as a function of temperature for various cell sizes (as indicated, in units of the fcc conventional unit cell lattice parameter) with $J' = 10^{-9}$ J/m and for a $10\times10\times10$ cell with $J' = 0$.

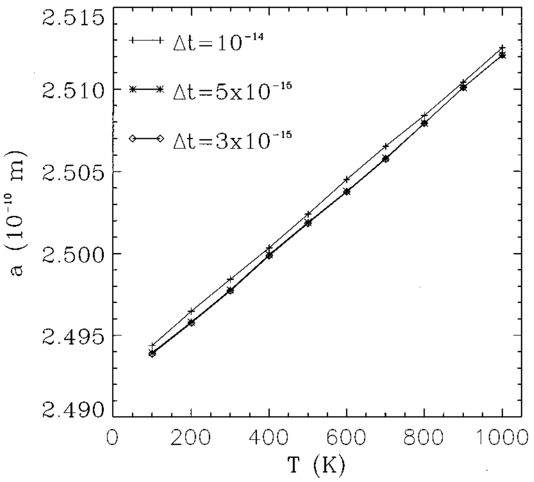

FIG. 3. Lattice parameter as a function of temperature for three different MD time steps (as indicated, in seconds).

cient accuracy of ~1% such that it was not necessary to use the cumulant intersection method.[40]

The dependence of T_C on J' suggests both that, when $J'\neq 0$, the magnetic short-range order (SRO) above T_C induces a significant magnetovolume expansion (or contraction if $J'<0$) and that relatively strong magnetic SRO above T_C is stabilized by the magnetovolume coupling. A large magnetic SRO-induced magnetovolume expansion is confirmed by our simulations, as shown in Fig. 6 where the average zero-pressure equilibrium lattice parameter a is plotted as a function of temperature for various values of J'. Here, in addition to the expected spontaneous magnetovolume expansion that sets in at T_C as temperature is lowered and that is strongly correlated to $\mu(T)$, we note a large magnetovolume expansion above T_C that extends far above T_C. This is emphasized in Fig. 7 where $(a-a_0)/a_0$ at zero pressure is plotted versus T/T_C for various values of J'. Here, a_0 is the value of $a(T)$ when $J'=0$.

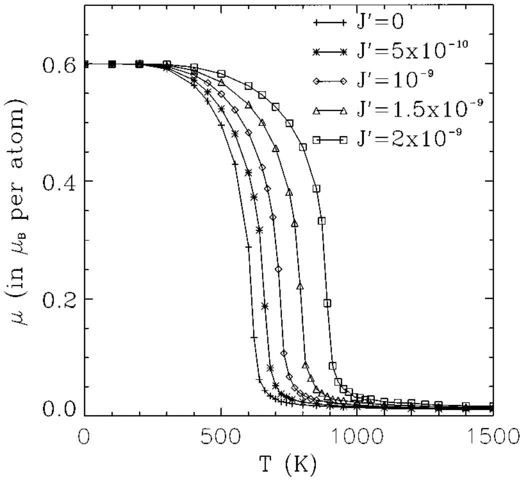

FIG. 4. Spontaneous average magnetic moment per atom as a function of temperature for various values of the magnetovolume coupling parameter J' (as indicated, in J/m), using a $10\times10\times10$ cell.

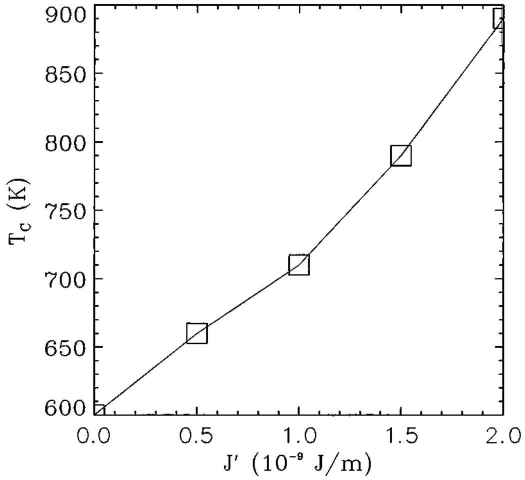

FIG. 5. Curie point, at zero pressure and zero applied magnetic field, as a function of J', using a $10\times10\times10$ cell.

The large magnetic SRO induced magnetovolume expansion above T_C shown in Figs. 6 and 7 has not previously been calculated. It is a demonstration that the validity of the usual practice of extrapolating the normal (i.e., $J'=0$) behavior from the paramagnetic state is tenuous and that this procedure is subject to large errors. It is also, therefore, a good example of the necessity of treating the magnetic and phonon degrees of freedom on an equal footing in ferromagnets with magnetovolume coupling.

The large magnetovolume expansion above T_C is not a finite-size-effect artifact, even though $\mu(T)$ exhibits unavoidable finite-size effects above T_C. This is demonstrated in Fig. 2. Neither the magnetic energy or the magnetovolume expansion show any detectable finite size effects for sizes $10\times10\times10$ or larger. Also, the fact that the large magnetovolume expansion above T_C is due to magnetic SRO is established by comparisons with simulations in which we impose perfectly random spin orientations (and exactly zero net magnetization) at the same temperatures above T_C (and with the same values of J').

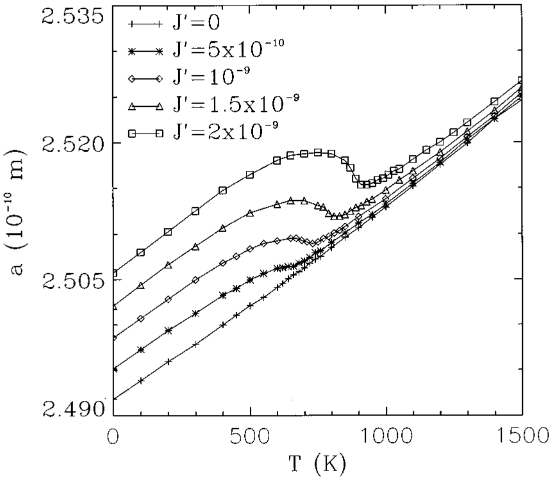

FIG. 6. Equilibrium lattice parameter as a function of temperature for various values of J' (as indicated, in J/m), using a $10\times10\times10$ cell.

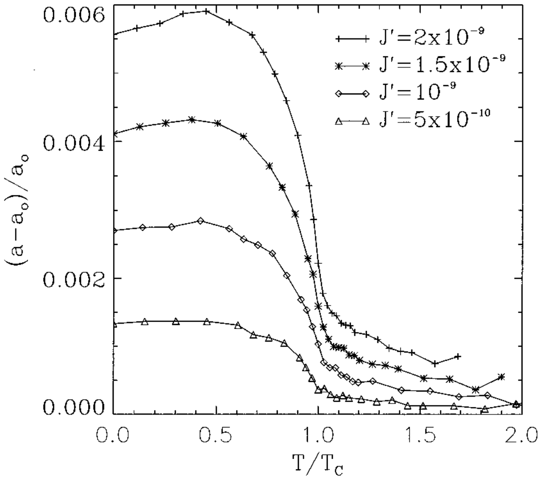

FIG. 7. Reduced equilibrium lattice parameter $[(a-a_0)/a_0$, where a_0 is the temperature-dependent equilibrium lattice parameter corresponding to $J'=0]$ as a function of reduced temperature (T/T_C) for various values of J' (as indicated, in J/m), using a $10\times10\times10$ cell.

This is shown in Fig. 8 where $a(T)$ is plotted (1) for $J'=0$, (2) for $J'=2\times10^{-9}$ J/m, and (3) for $J'=2\times10^{-9}$ J/m with an imposed random spin configuration and an imposed exactly zero net magnetization at each temperature. The large difference between the curve corresponding to spontaneous spin alignment and the other two curves establishes that magnetic SRO is the main cause of a large magnetovolume expansion above T_C that, here, persists to at least $T=1.7T_C$.

The smaller but systematic difference between the $J'=0$ curve and the $J'=2\times10^{-9}$ J/m and random spin configuration curve (Fig. 8) is real in that it is typically 2–4 times greater than the sum of the standard deviation errors for the two curves, at nonzero temperatures and for a size of $10\times10\times10$. Its authenticity is further established by simulations at $T=0$ K that are illustrated in Fig. 9. Here, $T=0$ K lattice parameters are shown that correspond to either $J'=0$ with a cell edge length of 10 (cell size of $10\times10\times10$) or $J'=2\times10^{-9}$ J/m with an imposed random spin configuration and imposed exactly zero net magnetization, as a function of the cell edge length. The error bars arise from considering several different random spin configurations for a given cell size.

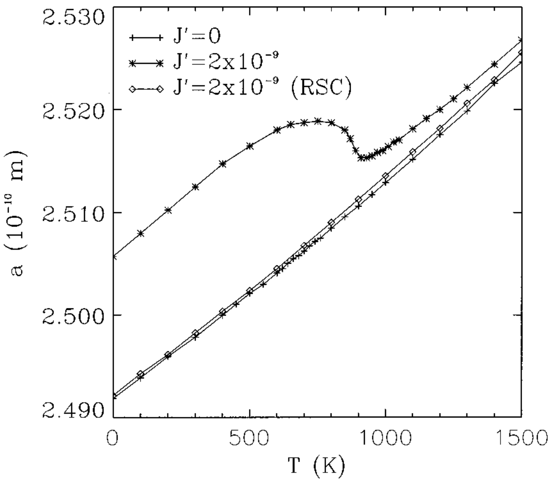

FIG. 8. Equilibrium lattice parameter as a function of temperature for three situations (as indicated) with equilibrium spin configuration and $J'=0$, with equilibrium spin configuration and $J'=2\times10^{-9}$ J/m, and with a perfectly random spin configuration (RSC) and $J'=2\times10^{-9}$ J/m.

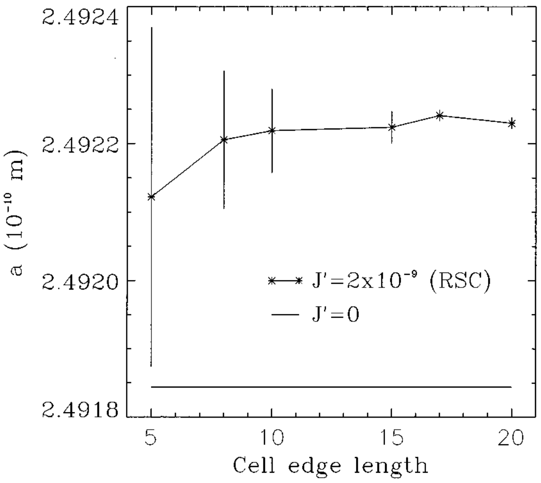

FIG. 9. The $T=0$ K equilibrium lattice parameters for $J'=2\times10^{-9}$ J/m and a perfectly random spin configuration (RSC) and for $J'=0$ (as indicated) as functions of the cubic simulation cell edge length (in units of the fcc conventional unit cell lattice parameter). The standard deviation error bars are based on several different perfectly random spin configurations for a given cell size.

This feature (i.e., the difference between the $J'=0$ lattice parameter and a $J'\neq0$ lattice parameter, in a perfectly random spin configuration state as must occur at $T\gg T_C$) does not occur in any mean-field or Landau-type calculation that imposes uniform lattice expansion rather than allow atomic-scale local variations in NN separation. Here, these local variations are induced by the long-lived spin disorder, via the nonzero J'. The observed difference (Figs. 8 and 9) also could not occur if the interatomic chemical potential were symmetric. This new effect, therefore, arises from the fluctuations in NN separation induced by long-lived spin disorder in the presence of an asymmetric interatomic potential. In real systems, it would not occur at temperatures or in cases where the on-site spin fluctuations might be as fast as or faster than the atomic vibrations.

Figure 10 shows the same data as in Fig. 4 but plotted as a function of T/T_C instead of T. Note that, in the neighborhood of but below T_C, the magnetic order parameter (μ) for larger values of J' is larger, within numerical accuracy, than for smaller values of J'. This suggests a nonuniversal behavior of $\mu(T/T_C)$, possibly with J'-dependent critical exponents and a transition that becomes first order for large enough J', in agreement with renormalization-group calculations.[38]

Our simulations also allow us to change the applied pressure. Figure 11 shows the $J'=10^{-9}$ J/m average magnetic moment per atom as a function of temperature, for different values of the applied hydrostatic pressure. A pressure of

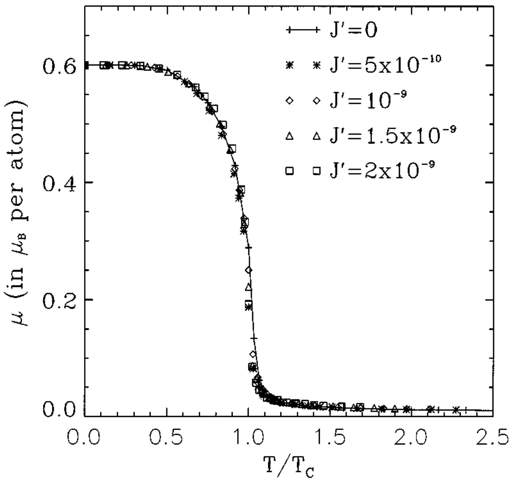

FIG. 10. Spontaneous average magnetic moment per atom as a function of reduced temperature (T/T_C) for various values of the magnetovolume coupling parameter J' (as indicated, in J/m), using a 10×10×10 cell.

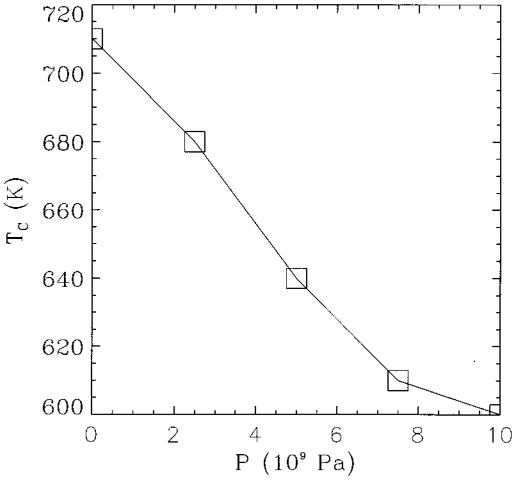

FIG. 12. Curie point as a function of the applied hydrostatic pressure, using a 10×10×10 cell and $J'=10^{-9}$ J/m.

10^{10} Pa is typical of what can be obtained in the laboratory, using diamond anvil cell technology. We note that, given the large and positive J', the average lattice parameter is decreased as pressure is increased and the corresponding Curie temperature is significantly decreased. This variation with pressure of the $J'=10^{-9}$ J/m T_C, obtained from the maximum in the specific heat, is shown in Fig. 12.

Figure 13 shows the same data as in Fig. 11 but plotted as a function of T/T_C instead of T. Here, we observe scaling of $\mu(T)$, within numerical accuracy, showing that applied pressure does not change the nature of the transition.

Finally, Fig. 14 shows $a(T)$ for different values of the pressure. Such curves directly give the bulk modulus, here for $J'=10^{-9}$ J/m, as a function of temperature. Zero-pressure bulk modulus curves $B(T)$ for different values of J' are shown in Fig. 15. Here, $B \equiv -V(\Delta P/\Delta V)$ where V is the $P=0$ sample volume and $\Delta P = 5\times 10^9$ Pa. One notes the main features that are observed in real ferromagnetic Invar alloys:[46] a broad and asymmetric trough that starts on the high-temperature side of T_C as temperature is lowered and that ends in a depressed value of B at magnetic saturation. The latter depression is approximately proportional to the value of J'.

V. CONCLUSION

We have presented a combined MD and MC approach for simulating the equilibrium properties of magnetovolume active local moment magnets. The approach is easily generalized to magnetic alloys with more than one moment-bearing species and with both chemical and spin disorder or to particular magnetic compounds having any type of spin structure. The only restriction is that the local moment autocorre-

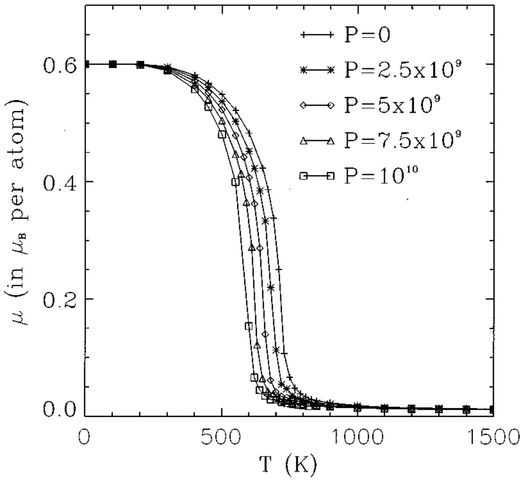

FIG. 11. Spontaneous average magnetic moment per atom as a function of temperature for various values of the applied hydrostatic pressure P (as indicated, in Pa), using a 10×10×10 cell and $J'=10^{-9}$ J/m.

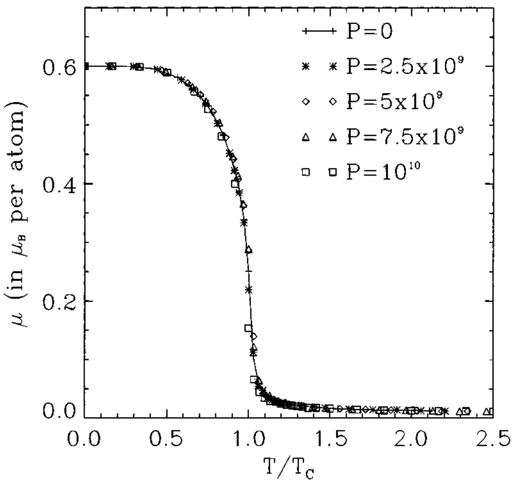

FIG. 13. Spontaneous average magnetic moment per atom as a function of reduced temperature (T/T_C) for various values of the applied hydrostatic pressure P (as indicated, in J/m), using a 10×10×10 cell and $J'=10^{-9}$ J/m.

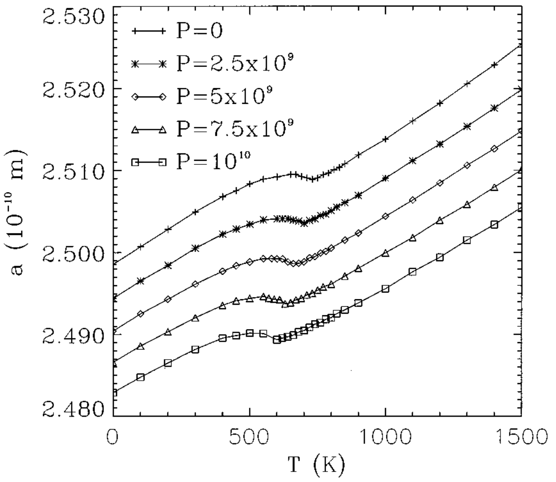

FIG. 14. Equilibrium lattice parameter as a function of temperature for various values of the applied hydrostatic pressure P (as indicated, in Pa), using a $10\times10\times10$ cell and $J'=10^{-9}$ J/m.

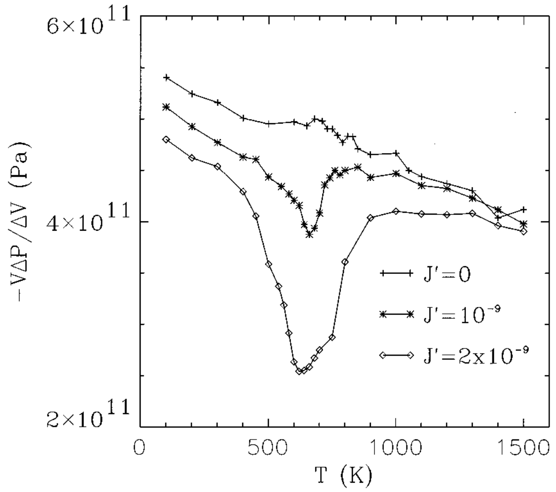

FIG. 15. Zero-pressure bulk modulus $B=-V(\Delta P/\Delta V)$, where V is the $P=0$ sample volume and $\Delta P=5\times10^9$ Pa, as a function of temperature for various values of J' (as indicated, in J/m) and using a $10\times10\times10$ cell.

lation times τ_m be much larger than typical periods τ_v of atomic vibrations (i.e., inverses of characteristic Debye or Einstein frequencies), as is often the case in real systems. This allows local average atomic positions to be used in calculating the effective exchange parameters seen by the magnetic moments, even though instantaneous interatomic separation-dependent exchange parameters are seen by the atoms as they execute their vibrations with a given (long-lived) spin configuration. As long as $\tau_m \gg \tau_v$, our algorithm should give correct equilibrium properties without any approximations other than the chosen model dependent ones (Ising interactions, NN interactions only, classical MD, etc.).

We have applied this approach to a simple model system which is a single-species local-moment ferromagnet with NN-only Lennard-Jones interatomic potential and NN-only Ising magnetic interactions. It is nickel-like in that it is fcc, has the same saturation moment per atom as nickel, the same $T=0$ K lattice parameter in the absence of magnetovolume coupling $(J'=0)$, the same Curie point when $J'=0$, and the same cohesive energy when $J'=0$. This sets all of the microscopic parameters except J'. The latter parameter is given various values large enough to induce spontaneous magnetovolume expansions comparable to those observed in strongly magnetovolume-coupled systems which, for example, are Fe-based metallic alloys such as $Fe_{65}Ni_{35}$ Invar.

All of the $J'=0$ simulated properties, such as ordinary thermal expansion, bulk modulus, and magnetic ordering, are in good agreement with those of metallic nickel and give a reliable base line for identifying the magnetovolume effects that occur when $J'\neq 0$. The main magnetovolume properties and effects evidenced by our simulations are (1) realistic thermal expansion curves $[a(T)$, Fig. 6] that have the same qualitative features as measured curves, including smooth tails above T_C and regions of zero or near-zero net thermal expansion, (2) magnetovolume coupling stabilized magnetic SRO that causes magnetovolume expansion far above T_C (Figs. 6–8), (3) a net true paramagnetic state (i.e., zero magnetic SRO) magnetovolume expansion (Figs. 8 and 9) that persists as long as $\tau_m \gg \tau_v$, (4) a significant dependence of T_C on J' (Fig. 5), (5) perturbed reduced magnetization versus reduced temperature curves (Fig. 10) that suggest a possible dependence of critical behavior on J', (6) accurately calculated effects of applied hydrostatic pressures (Figs. 11–14), and (7) realistic bulk modulus versus temperature curves (Fig. 15) that have the same qualitative features as measured curves, including large asymmetric troughs near T_C and negative saturation magnetovolume contributions.

This is the first combined MC-MD simulation to treat a magnetovolume-coupled magnetic system exactly at any temperature, applied field, and applied pressure. The vibrational and magnetic degrees of freedom are both allowed and they are coupled in a way that is consistent with the assumption that $\tau_m \gg \tau_v$. It is possible to relax this assumption or to consider the opposite limit of $\tau_m \ll \tau_v$ simply by changing the parameters of the simulation (n_{MD} and n_{MC}, Sec. II).

Three surprising results are found. The first is the extent to which magnetic SRO is enhanced by the magnetovolume coupling, leading to large magnetovolume expansions far above T_C. The second is the observation that, even in a true paramagnetic state with zero magnetic SRO, a net nonzero magnetovolume expansion occurs. The latter two points suggest a critical examination of the widespread practice of extrapolating measured values from the paramagnetic state $(T>T_C)$ in order to obtain the zero magnetovolume coupling behavior. Finally, the third surprising result is the suggestion that the critical behavior and the magnetic order parameter scaling are dependent on the strength of the magnetovolume coupling, in agreement with renormalization-group calculations.[38]

ACKNOWLEDGMENTS

We thank the Natural Sciences and Engineering Research Council of Canada for financial support.

*Author to whom correspondence should be addressed. Electronic address: dgr@physics.uottawa.ca

[1] M. Shiga, in *Materials Science and Technology*, edited by R.W. Cahn, P. Haasen, and E.J. Kramer (VCH, Weinheim, 1993), p. 159.

[2] M. Dubé, P.R.L. Heron, and D.G. Rancourt, J. Magn. Magn. Mater. **147**, 122 (1995).

[3] M.-Z. Dang, M. Dubé, and D.G. Rancourt, J. Magn. Magn. Mater. **147**, 133 (1995).

[4] M.-Z. Dang and D.G. Rancourt, Phys. Rev. B **53**, 2291 (1996).

[5] M.R. Ibarra, P.A. Algarabel, C. Morquina, J. Blasco, and J. Garcia, Phys. Rev. Lett. **75**, 3541 (1995).

[6] D.N. Argyriou, J.F. Mitchell, C.D. Potter, D.G. Hinks, J.D. Jorgensen, and S.D. Bader, Phys. Rev. Lett. **76**, 3826 (1996).

[7] Q. Shen, H. Luo, and J.K. Furdyna, Phys. Rev. Lett. **75**, 2590 (1995).

[8] E. Callen, J. Appl. Phys. **39**, 519 (1968).

[9] H. Sato, J. Appl. Phys. **29**, 456 (1958); Phys. Rev. **109**, 802 (1958).

[10] G.A. Alers, J.R. Neighbours, and H. Sato, J. Chem. Phys. Solids **13**, 40 (1960).

[11] G. Hausch, Phys. Status Solidi A **15**, 501 (1973).

[12] M.E. Lines, Solid State Commun. **22**, 75 (1977).

[13] E.R. Callen and H.B. Callen, Phys. Rev. **129**, 578 (1963); **139**, A455 (1965).

[14] R.C. O'Handley and C.-P. Chou, J. Appl. Phys. **49**, 1659 (1978).

[15] D. Bloch, J. Phys. Chem. Solids **27**, 881 (1966).

[16] E.W. Lee, Rept. Prog. Phys. **18**, 185 (1955).

[17] I.A. Campbell and G. Creuzet, in *Metallic Magnetism*, edited by H. Capellmann, (Springer-Verlag, Berlin, 1986), p. 207.

[18] A.J. Holden, V. Heine, and J.H. Samson, J. Phys. F **14**, 1005 (1984).

[19] T. Moriya and K. Usami, Solid State Commun. **88**, 911 (1993).

[20] C.P. Bean and D.S. Rodbell, Phys. Rev. **126**, 104 (1962).

[21] S. Fujiki, J. Magn. Magn. Mater. **31-34**, 101 (1983).

[22] A.Z. Menshikov, J. Magn. Magn. Mater. **5**, 188 (1977); **10**, 205 (1979).

[23] E.Z. Valiev and A.Z. Menshikov, J. Magn. Magn. Mater. **46**, 199 (1984).

[24] M.L. Plumer, J. Phys. C **19**, 6717 (1986).

[25] M.L. Plumer, Phys. Rev. B **44**, 12 376 (1991).

[26] M.L. Plumer, Phys. Rev. B **53**, 594 (1996).

[27] M.L. Plumer and A. Caillé, Phys. Rev. B **37**, 7712 (1988).

[28] M.L. Plumer, J. Phys. C **20**, 3029 (1987).

[29] M.L. Plumer, J. Phys. C **15**, 7181 (1982).

[30] M.B. Walker, Phys. Rev. B **22**, 1338 (1980).

[31] D.G. Rancourt, Solid State Commun. **58**, 433 (1986).

[32] K.G. Fischer and G. Heber, J. Magn. Magn. Mater. **62**, 181 (1986).

[33] M. Marchand, A. Caillé, and R. Pépin, Phys. Rev. B **34**, 4710 (1986); M. Marchand, K. Hood, and A. Caillé, Phys. Rev. Lett. **58**, 1660 (1987).

[34] J. Fivez, H. De Raedt, and B. De Raedt, Phys. Rev. B **21**, 5330 (1980).

[35] M. Barma, Phys. Rev. B **12**, 2710 (1975).

[36] B.K. Chakrabarti, N. Bhattacharyya, and S.K. Sinha, J. Phys. C **15**, L777 (1982).

[37] L. Gu, B. Chakraborty, P.L. Garrido, M. Phani, and J.L. Lebowitz, Phys. Rev. B **53**, 11 985 (1996), and references therein.

[38] D.J. Bergman and B.I. Halperin, Phys. Rev. B **13**, 2145 (1976), and references therein.

[39] N.W. Ashcroft and N.D. Mermin, *Solid State Physics* (Saunders College, Philadelphia, 1976).

[40] See, for example, K. Binder and D.W. Hermann, *Monte Carlo Simulations in Statistical Physics* (Springer-Verlag, Berlin, 1988).

[41] H.C. Andersen, J. Chem. Phys. **72**, 2384 (1980).

[42] J.M. Haile and H.W. Graben, J. Chem. Phys. **73**, 2412 (1980).

[43] See, for example, M.P. Allen and D. J. Tildesley, *Computer Simulations of Liquids* (Oxford University Press, New York, 1989).

[44] D. Brown and J.H.R. Clarke, Mol. Phys. **51**, 1243 (1984).

[45] D.G. Rancourt and M.-Z. Dang, this issue, Phys. Rev. B **54**, 12 225 (1996).

[46] G. Hausch and H. Warlimont, Z. Metallkd. **63**, 547 (1972).